Article

The Structure and Function of Quinones in Biological Solar Energy Transduction: A Cyclic Voltammetry, EPR, and Hyperfine Sub-Level Correlation (HYSCORE) Spectroscopy Study of Model Naphthoquinones

Christopher S. Coates,[†] Jessica Ziegler,[†] Katherine Manz,[†] Jacob Good,[†] Bernard Kang,[†] Sergey Milikisiyants,[†] Ruchira Chatterjee,[†] Sijie Hao,[‡] John H. Golbeck,[‡,§] and K. V. Lakshmi*,[†]

[†]Department of Chemistry and Chemical Biology and The Baruch '60 Center for Biochemical Solar Energy Research, Rensselaer Polytechnic Institute, Troy, New York 12180, United States

[‡]Department of Biochemistry and Molecular Biology, The Pennsylvania State University, University Park, Pennsylvania 16802, United States

[§]Department of Chemistry, The Pennsylvania State University, University Park, Pennsylvania 16802, United States

S *Supporting Information*
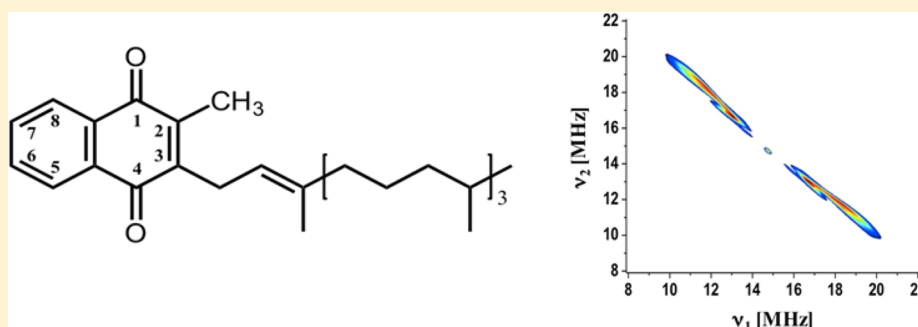
ABSTRACT: Quinones function as electron transport cofactors in photosynthesis and cellular respiration. The versatility and functional diversity of quinones is primarily due to the diverse midpoint potentials that are tuned by the substituent effects and interactions with surrounding amino acid residues in the binding site in the protein. In the present study, a library of substituted 1,4-naphthoquinones are analyzed by cyclic voltammetry in both protic and aprotic solvents to determine effects of substituent groups and hydrogen bonds on the midpoint potential. We use continuous-wave electron paramagnetic resonance (EPR) spectroscopy to determine the influence of substituent groups on the electronic properties of the 1,4-naphthoquinone models in an aprotic solvent. The results establish a correlation between the presence of substituent group(s) and the modification of electronic properties and a corresponding shift in the midpoint potential of the naphthoquinone models. Further, we use pulsed EPR spectroscopy to determine the effect of substituent groups on the strength and planarity of the hydrogen bonds of naphthoquinone models in a protic solvent. This study provides support for the tuning of the electronic properties of quinone cofactors by the influence of substituent groups and hydrogen bonding interactions.

INTRODUCTION

In photosynthesis and respiration, quinones are used for electron and proton transport, as these cofactors are highly tunable and versatile in function.[1–4] It is known that substituted benzoquinone and naphthoquinone molecules serve as electron acceptors in the type II reaction centers (RC), photosystem II (PSII) and the bacterial reaction center (BRC), and the type I RC, photosystem I (PSI), respectively.[5–14] The large difference in the redox potential of the benzoquinone and naphthoquinone cofactors in the RC proteins is thought to arise from a difference in the substituent groups on the quinone ring, hydrogen bonding (H-bonding) interactions, hydrophobic interactions, π-stacking with the surrounding protein environment, and the conformation of the phytyl chain of the

respective quinones.[15–21] Each of these factors acts in tandem to either stabilize or destabilize the semiquinone anion radical that is formed *in vivo*.

Phylloquinone, also known as vitamin K$_1$ (VK$_1$), is a substituted 1,4-naphthoquinone with a phytyl chain. Previous studies have suggested that the presence of different substituent groups on a 1,4-naphthoquinone molecule affect the electron spin density distribution on the quinone ring.[22–24] Quantum mechanical and molecular modeling methods have previously been used to examine the influence of the protein environment

and the effect of H-bonding interactions on the electron spin density distribution of quinones.[25,26] In addition, spectroscopic techniques, such as transient continuous-wave (cw) electron paramagnetic resonance (EPR) spectroscopy, Fourier transform infrared (FTIR) spectroscopy, and time-resolved absorption spectroscopy have been used to probe the interactions between quinones and their surrounding environment.[18,27−33]

In PSI, there are two highly symmetric phylloquinone molecules, A_{1A} and A_{1B}, that act as single electron acceptors. Although the phylloquinone molecules are chemically identical, A_{1A} and A_{1B} are functionally distinct (Figure 1). This is
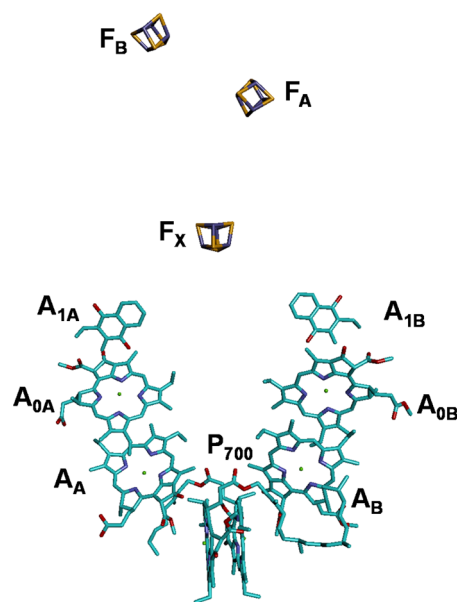
Figure 1. The electron-transfer cofactors in the A- and B-branches of photosystem I.

apparent in the lifetime of the reduced phyllosemiquinone anions, A_{1A}^{-} and A_{1B}^{-}, which is ∼200 and ∼20 ns, respectively.[34−37] The lifetime of the respective phyllosemiquinones is representative of the rate of electron transfer between the phylloquinone and the iron−sulfur cluster, F_x, through the A and B branches of PSI. One of the reasons for the distinct functional behavior of A_{1A} and A_{1B} is the difference in the midpoint potential of the cofactors. Recently, density functional theory, free energy, and electrostatic calculations have estimated the midpoint potential of A_{1A} and A_{1B} as −671 and −844 mV, respectively.[16] Given that A_{1A} and A_{1B} are identical phylloquinone molecules, it is proposed that interactions with the surrounding protein environment influence the electronic structure of the quinones.

The effect of the protein environment on the functional tuning of quinone cofactors has previously been studied by the biosynthetic replacement of the phylloquinone with plastoquinone in PSI.[38] In PSII, the primary plastoquinone is a one-electron acceptor operating at an estimated midpoint potential of ∼ −100 mV (vs NHE). When plastoquinone replaces the naturally occurring phylloquinone in PSI, the midpoint potential is shifted to −650 mV (vs NHE), a value far more similar to that of the native phylloquinone in PSI. These studies indicate that the protein environment directly affects the functional tuning of quinone cofactors. In addition to the protein environment, the effect of the presence of substituent

groups on quinone function has been studied by the replacement of the native phylloquinone of PSI with 2,3-dichloro-1,4-naphthoquinone (vs NHE).[39] The midpoint potential of 2,3-dichloro-1,4-naphthoquinone is ∼400 mV more positive than the native phylloquinone. Thus, when the native phylloquinone is replaced with 2,3-dichloro-1,4-naphthoquinone, the electron transfer pathway of PSI is blocked at the A_{1A} and A_{1B} sites.

In the present study, we perform a systematic investigation of an extensive library of substituted naphthoquinone models and phylloquinone (VK_1). We use cw EPR and two-dimensional (2D) hyperfine sublevel correlation (HYSCORE) spectroscopy to measure the isotropic and anisotropic components of the electron−nuclear hyperfine interactions of the substituted naphthoquinone models. From cw EPR spectroscopy, we obtain information on the isotropic component of the electron−nuclear hyperfine interaction that provides a direct measure of the electron spin density distribution on the individual carbon atoms of the reduced naphthosemiquinone models. Further, we elucidate the strength and geometry of H-bonds between the reduced naphthosemiquinones and a protic solvent using 2D HYSCORE spectroscopy. In parallel, we perform cyclic voltammetry measurements to determine the redox potentials of the naphthoquinone models in both protic and aprotic solvents. We correlate the electron spin density distribution of the naphthosemiquinone models that is obtained by cw EPR and 2D HYSCORE spectroscopy with the substituent and solvent effects and relate these to the midpoint potential of the naphthoquinone models. This study provides valuable insight on the influence of molecular interactions on the tuning and function of quinones *in vitro*.

■ MATERIALS AND METHODS

Preparation of Naphthosemiquinone Anion Radicals. 1,4-Naphthoquinone (NQ), 5-hydroxy-1,4-naphthoquinone (5-OHNQ), and 2,3-dichloro-1,4-naphthoquinone (DCNQ) were obtained from Aldrich Chemical Co., Inc. (Milwaukee, WI). 2-Methyl-1,4-naphthoquinone (MNQ) was obtained from Nutritional Biochemicals Corporation (Cleveland, OH), and vitamin K_1 (VK_1) was obtained from Alfa Aesar (Ward Hill, MA). The numbering scheme of the carbon atoms of the naphthoquinone models is shown in Figure 2.

The naphthosemiquinone anion radicals were generated by dissolving the naphthoquinone models (0.2−10 mM) in dimethyl sulfoxide (DMSO) (Mallinckrodt Chemicals, Phillipsburg, NJ) or isopropyl alcohol (IPA) (J. T. Baker, Phillipsburg, NJ) in a Bactron X anaerobic chamber (Sheldon Manufacturing Inc., Cornelius, OR). The naphthosemiquinone anion radicals in DMSO were generated by adding 1.0 M sodium hydroxide (NaOH) dropwise, and the naphthosemiquinone radicals in IPA were generated using potassium tertiary buteroxide (*t*-BtOx) (Sigma-Aldrich, St. Louis, MO). The VK_1 semiquinone anion radical was formed using one drop of benzyltrimethylammonium hydroxide in 40% methanol (Sigma-Aldrich, St. Louis, MO). For the cw EPR spectroscopy measurements at room temperature, the naphthosemiquinone samples were loaded into 2 mm glass capillaries (Kimble Chase, Vineland, NJ) and placed in 4 mm quartz tubes (Wilmad LabGlass, Vineland, NJ). For the cryogenic pulsed X-band 2D HYSCORE spectroscopy measurements, the naphthosemiquinone models were loaded into 4 mm quartz tubes and frozen at 77 K.

Electrochemical Measurements. Cyclic voltammetry (CV) measurements were performed on a bipotentiostat
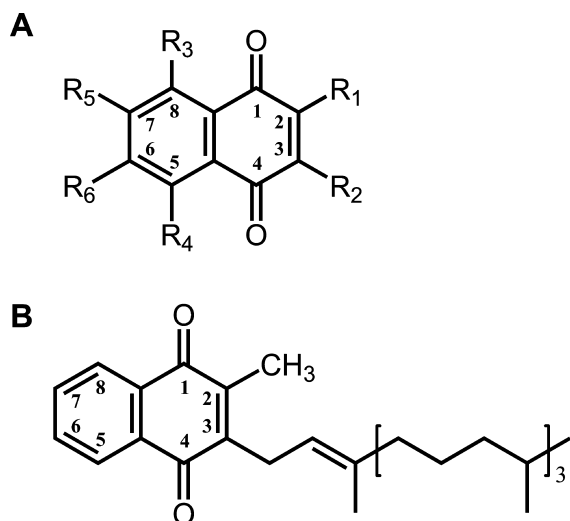
Figure 2. The structure of (A) naphthoquinone models (**NQ** $R_1 = R_2 = R_3 = R_4 = R_5 = R_6 = H$; **MNQ** $R_1 =$ methyl, $R_2 = R_3 = R_4 = R_5 = R_6 = H$; **ENQ** $R_1 =$ ethyl, $R_2 = R_3 = R_4 = R_5 = R_6 = H$; **DMNQ** $R_1 = R_2 =$ methyl, $R_3 = R_4 = R_5 = R_6 = H$; **5-OHNQ** $R_1 = R_2 = R_3 = R_5 = R_6 = H$, $R_4 =$ hydroxyl; **DCNQ** $R_3 = R_4 = R_5 = R_6 = H$, $R_1 = R_2 =$ chloro) and (B) vitamin VK₁ (VK₁).

(model AFCBP1) (Pine Instrument Company, Grove City, PA) using a three-electrode system consisting of a glassy carbon working electrode, a platinum wire counter electrode, and a silver wire reference electrode. The CV measurements of the naphthoquinone models in dry acetonitrile were performed with 0.1 M tetrabutylammonium hexaflourophosphate (TBAPF₆) as the supporting electrolyte (Indofine Chemical Company Inc., Hillsborough, NJ). In addition, CV measurements of the naphthoquinone models were also performed in dry ethanol with 0.1 M sodium perchlorate (NaClO₄) as the supporting electrolyte (Alfa Aesar, Heysham, Lancashire, U.K.). The concentration of the samples was between 2 and 3 mM, varying based on the solubility of the naphthoquinone. The measurements were performed in an argon atmosphere at 25 °C, and ferrocene (Sigma-Aldrich, St. Louis, MO) that was purified by sublimation was used as an internal standard for the measurements. All of the CV measurements are referenced to ferrocene/ferrocinium (Fc/Fc⁺) and corrected to the normal hydrogen electrode (NHE) (Fc = 0.400 V vs aqueous SCE in acetonitrile; Fc = 0.456 V vs aqueous SCE in ethanol; SCE = −0.24 V vs NHE).[40−42] The cyclic voltammograms were plotted in Origin 8.0 where the redox potentials were calibrated by referencing the Fc/Fc⁺ internal standard to the NHE standard potential. The midpoint was determined by averaging the values of the cathodic and anodic peak potentials.

CW and Pulsed EPR Spectroscopy. The EPR spectra were obtained on a custom-built cw/pulsed X-band Bruker Elexsys 580 EPR spectrometer. The cw EPR measurements were performed at room temperature using a dual-mode resonator ER 4116-DM (Bruker BioSpin, Billerica, MA) equipped with a continuous-flow helium E900 cryostat (Oxford Instruments, Oxfordshire, U.K.). The operating microwave frequency was 9.64 GHz. The EPR spectra were acquired using a modulation frequency of 100 kHz and modulation amplitude of 0.05−0.1 G. The experimental cw EPR spectra that were acquired at room temperature were simulated using the "*garlic*" spectral subroutine of the EasySpin software package. This

subroutine is designed to reproduce isotropic cw EPR spectra on a Matlab R2010b platform.[43]

The pulsed EPR spectroscopy measurements were obtained using a dielectric flex-line ER 4118-MD5 probe (Bruker BioSpin, Billerica, MA) and a dynamic continuous-flow cryostat CF935 (Oxford Instruments, Oxfordshire, U.K.). An operating microwave frequency of 9.71 GHz was used for the pulsed resonator. The 2D HYSCORE spectra were recorded at a magnetic field position of 3458 G. The pulsed EPR spectra were recorded at 115 K.

For the 2D HYSCORE spectra, the pulsed echo amplitude was measured using the sequence $\pi/2\text{-}\tau\text{-}\pi/2\text{-}t_1\text{-}\pi\text{-}t_2\text{-}\pi/2\text{-echo}$ with a τ value of 132 ns and a 12 ns detector gate (centered at the maximum of the echo signal); the delays are defined as the differences in the starting points of the pulses. The echo intensity was measured as a function of t_1 and t_2, where t_1 and t_2 were incremented in steps of 8 or 16 ns from their initial values of 24 and 40 ns, respectively. Equal amplitude pulses of 16 ns for $\pi/2$ and 32 ns for π were used to record a 256 × 256 matrix. The 16 ns time difference between the initial values of t_1 and t_2 and $\pi/2$ and π were set equal to obtain more symmetric spectra. The unwanted echoes and anti-echoes were eliminated by applying a 16-step phase cycling procedure.[44]

For the 2D HYSCORE data, a low-order polynomial baseline correction and tapering with a Hamming function was used to remove the unwanted echo decay. Before the application of a 2D Fourier transform, the data was zero filled to a 1024 × 1024 matrix and the magnitude spectra were calculated using the Bruker X-EPR software (Bruker BioSpin, Billerica, MA). The 2D HYSCORE spectral contour plots were created using Matlab R2010b.

Theory and Analysis. The isotropic hyperfine coupling parameters were obtained by spectral simulation of the room-temperature cw EPR spectra of the naphthosemiquinone models. The corresponding electron spin density distribution at each of the carbon atoms of the naphthosemiquinone models was calculated using the McConnell relationship.[45] The McConnell relationship for the calculation of the electron spin density on the carbon atoms that are adjacent to α-protons is

$$a_N = Q\rho_N \tag{1}$$

where a_N is the isotropic hyperfine interaction for the nucleus, N, ρ_N is the electron spin density at the α carbon atom that is adjacent to the nucleus, N, and Q is a constant. For 1,4-naphthoquinone, the value of Q for the α protons that are directly bound to the naphthoquinone ring is −27 G.[46] For methyl and ethyl protons, the value of Q is 20 and 26 G, respectively.[47,48]

The electron spin density distribution at each carbon atom of VK₁ was calculated using the complete McLachlan relationship which takes into account the angle of the β-methylene protons of the phytyl chain with respect to the plane of the naphthoquinone ring:[48]

$$a_N = (B_o + B_1 \cos^2(\theta)\rho_N) \tag{2}$$

Here, B_o is a constant approximated to zero and B_1 is 112 MHz.[49]

The three principal components of an electron−nuclear hyperfine tensor can be represented as $(A_x, A_y, A_z) = (a_{iso} - T(1 - \delta), a_{iso} - T(1 + \delta), a_{iso} + 2T)$, where a_{iso}, T, and δ are the isotropic, dipolar, and rhombic components of the

hyperfine tensor, respectively. In the case of axial symmetry ($\delta = 0$, $A_x = A_y = A_\perp = a_{iso} - T$, $A_z = A_\parallel = a_{iso} + 2T$), the proton cross-peaks (which appear as ridges in powder samples) represent straight-line segments when plotted in frequency-squared coordinates. In this case, the anisotropic and isotropic components of the electron−nuclear hyperfine interaction can be obtained from the slope and intercept of the ridges. On the basis of the value of the slope, $Q_{\alpha(\beta)}$, and intercept, $G_{\alpha(\beta)}$, that are determined experimentally and the calculated value of the nuclear Zeeman frequency, v_I, the value of a_{iso} and T can be calculated from the following equations:[50]

$$T = \pm \sqrt{\frac{16}{9(1 - Q_{\alpha(\beta)})}\left\{G_{\alpha(\beta)} + \frac{4v_I^2 Q_{\alpha(\beta)}}{1 - Q_{\alpha(\beta)}}\right\}} \quad \text{and}$$

$$a_{iso} = \pm 2v_I \frac{1 + Q_{\alpha(\beta)}}{1 - Q_{\alpha(\beta)}} - \frac{T}{2} \tag{3}$$

To obtain the value of $Q_{\alpha(\beta)}$ and $G_{\alpha(\beta)}$, the frequency-squared coordinates of the points were measured on the median of a ridge corresponding to the highest signal intensity along the direction of the ridges. This is appropriate, since the processes responsible for line broadening in the 2D frequency space (e.g., nuclear relaxation, hyperfine strain, and signal apodization) would not affect the position of maximum signal intensity. The measured coordinates were fit with a straight line using a least-squares algorithm that yielded the value of $Q_{\alpha(\beta)}$ and $G_{\alpha(\beta)}$. Each pair of $Q_{\alpha(\beta)}$ and $G_{\alpha(\beta)}$ values results in four sets of possible hyperfine parameters (please see eq 3), where the sign of T can be positive or negative and, for a given value of T, there are two possible values of a_{iso}.

In cases of significant rhombicity, the parameter δ causes the splitting of the ridge into two ridges that could be resolved in the experiment. For each of the two ridges, one can determine corresponding values of $A_\parallel$ and $A_\perp$, using the procedure described above. If indeed two ridges originate from a rhombic proton and not from two distinct protons with axial interactions, the value of $A_\perp$ will be identical within experimental deviations and provide a measure of the A_Z component of the rhombic hyperfine tensor. Two distinct values of $A_\parallel$ provide a measure of A_X and A_Y. Thus, all three principal values of the hyperfine tensor can be determined in a similar way in the case of axial symmetry.

■ RESULTS

Electrochemical Studies of Naphthoquinone Models. In this study, both aprotic (acetonitrile) and protic (ethanol) solvents were used for the CV measurements. The protic solvent, ethanol, forms hydrogen bonds (H-bonds) with the naphthoquinone models that are absent in the aprotic solvent, acetonitrile. This allows for the determination of the effects solely due to the presence of H-bonds on the redox potential of the respective naphthoquinone models. The cyclic voltammo-grams of the naphthoquinone models in acetonitrile and ethanol are shown in Figures 3 and 4, respectively. The cyclic voltammograms are referenced to the internal standard, Fc/Fc+. To facilitate qualitative visual comparison, a dashed line marks the midpoint potential of ferrocene. The reduction and oxidation couples of the naphthoquinone models have been obtained by averaging the maximum and minimum voltages in the cyclic voltammogram.
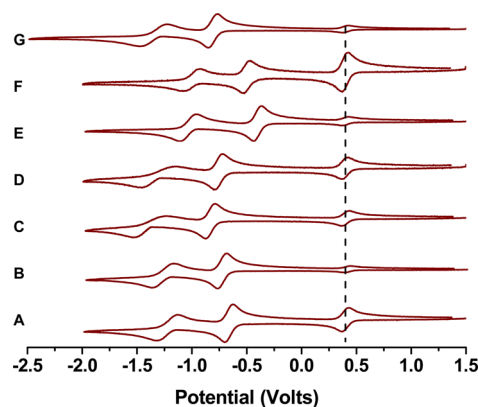
Figure 3. The cyclic voltammogram of naphthoquinone models in acetonitrile that are referenced to ferrocene (0.40 V vs NHE; represented by the dashed line): (A) 1,4 NQ; (B) MNQ; (C) DMNQ; (D) ENQ; (E) DCNQ; (F) 5-OHNQ; (G) VK₁.
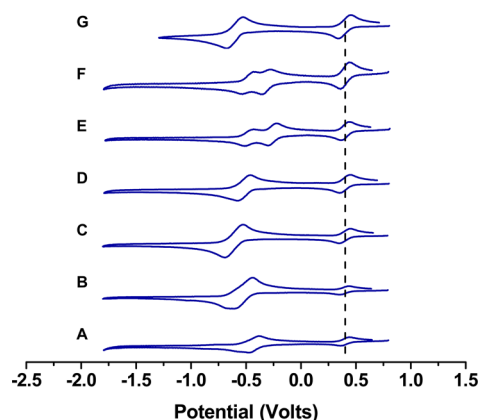
Figure 4. The cyclic voltammogram of the naphthoquinone models in ethanol that are referenced to ferrocene (0.456 V vs NHE; represented by the dashed line): (A) 1,4-NQ; (B) MNQ; (C) DMNQ; (D) ENQ; (E) DCNQ; (F) 5-OHNQ; (G) VK₁.

The values of the midpoint potential of the naphthoquinone models in acetonitrile and ethanol are presented in Table 1.

Table 1. The First Mid-Point Potential of the Naphthoquinone Models vs NHE in Acetonitrile and Ethanol, Respectively

	midpoint potential (V)	
quinone (abbreviation)	in ethanol	in acetonitrile
1,4-naphthoquinone (NQ)	−0.610	−0.903
2,3-dichloro-1,4-naphthoquinone (DCNQ)	−0.445	−0.644
5-hydroxy-1,4-naphthoquinone (5-OHNQ)	−0.503	−0.735
2-methyl-1,4-naphthoquinone (MNQ)	−0.715	−0.981
2-ethyl-1,4-naphthoquinone (ENQ)	−0.701	−1.002
2,3-dimethyl-1,4-naphthoquinone (DMNQ)	−0.795	−1.070
vitamin K₁ (VK₁)	−0.786	−1.049

The substituent groups on the naphthoquinone ring affect the value of the midpoint potential in both solvents. There is a decrease in the midpoint potential (to a more negative value) of the naphthoquinones in the presence of electron-donating alkyl groups on the quinone ring. In contrast, there is an increase in the midpoint potential (to a more positive value) in the presence of electron-withdrawing groups (e.g., hydroxyl and

chloro substituents). For all of the naphthoquinone models, there is an increase in the midpoint potential in the presence of H-bonding interactions with the solvent. This is reflected by the more positive value of the midpoint potential of the naphthoquinone models in ethanol in comparison with the corresponding value of the midpoint potential that is measured in acetonitrile.

CW EPR Spectroscopy of Naphthoquinone Models. Shown in Figure 5 are the experimental (black trace) and
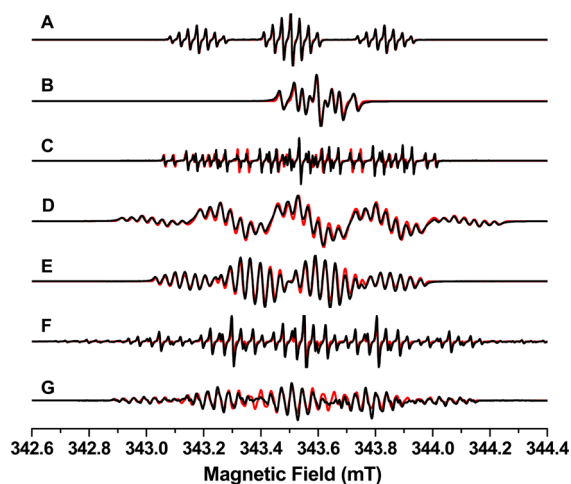

Figure 5. The experimental (black trace) and simulated (red trace) cw EPR spectra of naphthosemiquinone anion radicals in DMSO: (A) NQ; (B) DCNQ; (C) 5-OHNQ; (D) MNQ; (E) ENQ; (F) DMNQ; (G) VK$_1$.

simulated (red trace) cw EPR spectra of the naphthosemiquinone models at room temperature in DMSO. The cw EPR spectra display distinct line shape splitting patterns that are characteristic of the electron–nuclear hyperfine interactions between the electron spin ($S = 1/2$) on the naphthosemiquinone anion and the protons (nuclear spin, $I = 1/2$) that are in close proximity and magnetically interacting with the electron spin. In solution, rapid rotational reorientation of the molecules averages the anisotropic component of the hyperfine interaction. The only remaining directionally independent isotropic hyperfine component, a_{iso}, arises from the presence of electron spin density on the protons. The spectral splitting patterns that are observed in the cw EPR spectra of the naphthosemiquinone anion radical depend on the magnitude of the isotropic hyperfine interaction, a_{iso}, and the number of interacting protons. In this study, the experimental cw EPR spectra were numerically simulated to obtain the values of a_{iso}

(Table 2). The assignments of the isotropic hyperfine components are based on simple structural considerations and comparison with previous literature.[23]

2D ^{1}H HYSCORE Spectroscopy of Naphthoquinone Models. Figure 6 shows the ^{1}H HYSCORE spectrum of 1,4-
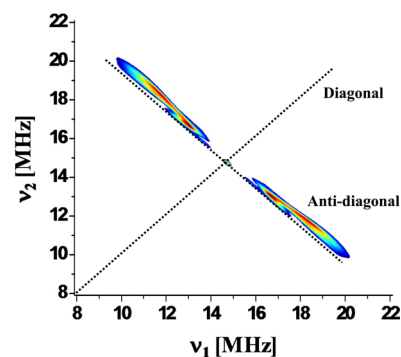
Figure 6. The 2D ^{1}H HYSCORE spectrum of 1,4-NQ in IPA.

naphthoquinone in IPA. As can be seen in this spectrum, the cross-peaks form extended ridges that are centered at the Zeeman frequency of the protons (14.72 MHz). The ridges arise from the hyperfine interactions between the electron spin ($S = 1/2$) of naphthosemiquinone anion and the protons ($I = 1/2$) that are in close proximity, such as the ring, substituent, and H-bonded protons.

The hyperfine interaction is characterized by two parameters, namely, the isotropic and anisotropic component, a_{iso} and T, respectively. The isotropic hyperfine component, a_{iso}, is a measure of the presence of electron spin density on the nucleus. The anisotropic hyperfine component, T, is due to a through-space dipolar interaction between the electron spin and the magnetic nucleus. The location of the ridges in the 2D frequency space in the HYSCORE spectrum is determined by the magnitude and the relative sign of a_{iso} and T. Qualitatively, a_{iso} causes separation of the observed ridges from the main diagonal that is defined as $\nu_1 + \nu_2 = 2\nu_p$, where ν_i is the proton Zeeman frequency. The anisotropic component, T, extends the ridges approximately along the antidiagonal that is defined as $\nu_1 = \nu_2$. Additionally, T causes a small shift of the ridges from the antidiagonal toward higher frequencies. Both the diagonal and antidiagonal have been marked on the 2D ^{1}H HYSCORE spectra in Figure 6.

In this study, we have determined both the isotropic and anisotropic components of the hyperfine interaction, a_{iso} and T, from linear analysis of the 2D ^{1}H HYSCORE spectra in frequency-squared coordinates (Figures S4–S10, Supporting

Table 2. The Isotropic Hyperfine Interaction Parameters of the Naphthoquinone Models That Are Obtained from the Numerical Simulations of the cw EPR Spectra in DMSO

| quinone (abbreviation) | a_{iso} (MHz) | | | | | |
	R_1	R_2	R_3	R_4	R_5	R_6
1,4-naphthoquinone (NQ)	9.20	9.20	0.87	0.87	1.75	1.75
2,3-dichloro-1,4-naphthoquinone (DCNQ)	n/a	n/a	1.47	1.47	2.18	2.18
5-hydroxy-1,4-naphthoquinone (5-OHNQ)	11.10	7.25	2.25	0.95	2.86	2.11
2-methyl-1,4-naphthoquinone (MNQ)	7.71	7.45	1.10	0.80	1.80	2.05
2-ethyl-1,4-naphthoquinone (ENQ)	6.37	7.40	1.05	0.80	1.80	2.10
2,3-dimethyl-1,4-naphthoquinone (DMNQ)	7.11	7.11	0.89	0.89	2.10	2.10
vitamin K$_1$ (VK$_1$)	7.20	4.40	3.10	0.80	1.00	2.10	1.80

Information). The values of a_{iso} and T that are obtained for the H-bonded protons are shown in Table 3. Due to decreased

Table 3. The Anisotropic Hyperfine Interaction Parameters of the H-Bonded Proton of the Naphthoquinone Models That Are Obtained from the 2D ^{1}H HYSCORE Spectra in the Protic Solvent, IPA

quinone (abbreviation)	A_{iso} (MHz)	T (MHz)
1,4-napthoquinone (NQ)	−0.11	2.86
2,3-dichloro-1,4-naphthoquinone (DCNQ)	−0.40	3.03
5-hydroxy-1,4-naphthoquinone (5-OHNQ)	0.21	2.83
2-methyl-1,4-naphthoquinone (MNQ)	−0.35	2.69
2-ethyl-1,4-naphthoquinone (ENQ)	∼0	2.81
2,3-dimethyl-1,4-naphthoquinone (DMNQ)	−1.91	4.30
vitamin K$_1$ (VK$_1$)	−2.16	4.37

orbital overlap between the carbonyl oxygen and the H-bonding proton, there is a low probability of finding unpaired electron spin density on the H-bonded proton. This leads to a much smaller value of a_{iso}. As can be seen in Table 3, the values of T and a_{iso} for the H-bonded protons are similar in the series of substituted naphthoquinone models, with an average anisotropic coupling constant of 2.84 MHz and negligible isotropic coupling constants. However, for DMNQ and VK$_1$, we observe much larger values of T of ∼4.3−4.4 MHz. Moreover, for both DMNQ and VK$_1$, the H-bonded protons have a larger value of a_{iso}, namely, 1.91 and 2.16 MHz for DMNQ and VK$_1$, respectively (the 2D ^{1}H HYSCORE spectra are shown in Figure S3, Supporting Information). We also determine the hyperfine parameters for the ring protons at positions 2 and 3 and the methyl protons in the case of the substituted naphthoquinone models. Additionally, for some of the ring protons, we resolve a small rhombic hyperfine component that provides the three principal components of the corresponding hyperfine tensor. The values of A_X, A_Y, and A_Z are displayed in Table 4. The weak interactions with the ring protons of the naphthoquinone models at positions 5−8 could not be resolved in the 2D ^{1}H HYSCORE spectra.

■ DISCUSSION

Electrochemical Studies of Naphthoquinone Models. The redox potential is a measure of the propensity of a molecule to either lose or gain an electron to its environment.

Table 4. The Hyperfine Interaction Parameters of the Ring Protons of the Naphthoquinone Models That Are Obtained from the 2D ^{1}H HYSCORE Spectra in the Protic Solvent, IPA

quinone (abbreviation)	A_X, A_Y, A_Z (MHz)
1,4-napthoquinone (NQ)	−14.2, −12.3, −2.4[a]
2,3-dichloro-1,4-naphthoquinone (DCNQ)	N/A
5-hydroxy-1,4-naphthoquinone (5-OHNQ)	−14.1, −11.7, −2.2[a]
2-methyl-1,4-naphthoquinone (MNQ)	(I) −12.4, −10.9, −2.1[a]; (II) 6.1, 6.1, 9.9[b]
2-ethyl-1,4-naphthoquinone (ENQ)	−11.3, −11.3, −1.5[a]
2,3-dimethyl-1,4-naphthoquinone (DMNQ)	5.4, 5.4, 9.7[b]
vitamin K$_1$ (VK$_1$)	-

[a]Ring proton. [b]Methyl group on the ring.

In cyclic voltammetry, a potential field is linearly swept where the sample is first reduced and then subsequently oxidized during the measurement. This manifests as separate peaks in the cyclic voltammogram that represent the reduction and oxidation of the quinone molecule. The midpoint potential of the quinone is determined by taking the average value of the two peaks. The presence of substituent groups on the ring directly affects the electronic structure of the naphthoquinone. An increase in the electron density on the carbonyl group of a quinone due to the presence of an electron-donating substituent group leads to increased electron repulsion. This leads to a negative shift in the midpoint potential. In contrast, the presence of an electron-withdrawing substituent group gives rise to a positive shift in the midpoint potential of the quinone. Similarly, the presence of H-bonds to the carbonyl oxygen atoms withdraws electron density from the quinone molecule that leads to a positive shift in the midpoint potential of the quinone.

Shown in Table 1 are the midpoint potentials of the naphthoquinone models. In comparison with the midpoint potential of 1,4-naphthoquinone, the substituted naphthoquinone models with electron-withdrawing groups, such as chloro and hydroxyl, display a more positive midpoint potential. In contrast, the naphthoquinone models with electron-donating groups, such as alkyl chains, display a more negative midpoint potential. In addition, it is observed that in the case of electron-donating substituent groups, after the initial addition of an alkyl substituent, the extension of the group from methyl, ethyl, to the phytyl substituent of VK$_1$ has little effect on the midpoint potential. However, the number of substituent groups has a pronounced effect on the midpoint potential as observed for DMNQ and VK$_1$. This indicates a strong effect on the value of the midpoint potential from the number of substituent groups directly bound to the quinone ring and a much weaker effect from the length of the substituent group. For electron-withdrawing substituent groups, the more electronegative atom in a substituent group is expected to display the largest effect on the midpoint potential of the quinone. This suggests that a hydroxyl substituent would have the largest effect on the midpoint potential of the naphthoquinone. However, upon comparison of 5-hydroxy-1,4-naphthoquinone (5-OHNQ) with 2,3-dichloro-1,4-naphthoquinone (DCNQ), the presence of the hydrogen in a hydroxyl group mitigates some of the electronegativity of the oxygen. In addition, there are two chlorine atom substituents in DCNQ in comparison with a single hydroxyl group in 5-OHNQ that causes two chlorine atoms to have a larger effect on the electron density of the naphthoquinone.

In addition to the presence of substituent groups, we also investigate the effect of H-bond interactions on the midpoint potential of the naphthoquinone models. In the presence of a protic solvent, ethanol, in addition to substituent effects, there are effects from the presence of H-bonds between the carbonyl group of the naphthoquinone and the solvent. The presence of H-bonds withdraws electron density from the naphthoquinone. Similar to the observation with the electron-withdrawing substituents, the presence of H-bonds causes a positive shift in midpoint potential of the naphthoquinone models. As displayed in Table 1, the values of the midpoint potential of the naphthoquinone models are shifted to more positive values in ethanol as compared to the values that are obtained in acetonitrile. This shift in the midpoint potential is greater for the alkyl-substituted naphthoquinone models (MNQ, ENQ,

DMNQ, and VK$_1$) than for those with electron-withdrawing substituents (DCNQ and 5-OHNQ). This is consistent with previous literature and is due to the relative basicity of the substituents.[51,52] The presence of electron-donating substituent groups increases the electron density on the carbonyl oxygen atom, which causes strong H-bonding interactions with the protic solvent.

The naphthoquinones with electron-withdrawing substituents, DCNQ and 5-OHNQ, display a smaller positive shift in the second midpoint potential in ethanol, while the naphthoquinones with alkyl substituents display only one cyclic wave (Figure 4). A similar trend has previously been observed with the addition of ethanol to benzonitrile in a study on benzoquinones. Previous CV measurements in water, methanol, and ethanol have also shown a positive shift in the second redox potential of quinones, caused by rapid H-bond equilibrium upon quinone reduction, resulting in a singular wave. The relative basicity of the quinone also affects this equilibrium, with a smaller effect observed for less basic quinones like DCNQ and 5-OHNQ.[53,54]

CW EPR Spectroscopy of Naphthoquinone Models. In a highly conjugated π-system, such as the naphthosemiquinone models, the electron spin density is distributed over the carbon and oxygen atoms of the primary ring of the molecule. The strength of the electron−nuclear hyperfine interaction is proportional to the electron spin density at the adjacent carbon atom on the aromatic ring. Using the proton hyperfine interactions that are displayed in Table 2, we calculate the electron spin density distribution on the carbon atoms of the naphthoquinone models (please see the Theory and Analysis section for details). The electron spin density distribution on the carbon atoms of the naphthosemiquinone models is presented in Table 5. In the present study, we describe the

Table 5. The Electron Spin Density Distribution of the Naphthoquinone Models That Are Obtained from the Spectral Simulations of cw EPR Spectra in the Aprotic Solvent, DMSO

quinone (abbreviation)	electron spin density (%)					
	C$_2$	C$_3$	C$_6$	C$_7$	C$_5$	C$_8$
1,4-naphthoquinone (NQ)	12.16	12.16	2.31	2.31	1.15	1.15
2,3-dichloro-1,4-naphthoquinone (DCNQ)	n/a	n/a	2.88	2.88	1.94	1.94
5-hydroxy-1,4-naphthoquinone (5-OHNQ)	14.68	9.59	2.79	3.78	n/a	2.78
2-methyl-1,4-naphthoquinone (MNQ)	13.76	9.85	2.71	2.38	1.06	1.46
2-ethyl-1,4-naphthoquinone (ENQ)	8.74	9.78	2.78	2.38	1.06	1.39
2,3-dimethyl-1,4-naphthoquinone (DMNQ)	12.69	12.69	2.78	2.78	1.17	1.17
vitamin K$_1$ (VK$_1$)	12.85	9.00^a	2.38	2.78	1.32	1.06

^{a}Niklas et al., 2009.[65]

numbering scheme of the naphthosemiquinone models using the nomenclature described in Figure 2. The 1,4-naphthoquinone molecule will be used as a standard for the comparison of substituted naphthoquinone models.

The experimentally determined electron spin density distribution of the naphthosemiquinone models in DMSO is

shown in Table 5. In 1,4-naphthoquinone, the majority of the electron spin density resides on the carbons atoms at the 2 and 3 positions of the primary ring and the carbonyl oxygen atoms.[23,55] A smaller percentage of the electron spin density is present on the carbon atoms at the 6 and 7 positions of the primary ring. The carbon atoms at the 5 and 8 positions have approximately half of the electron spin density in comparison with the carbon atoms at the 6 and 7 positions. This is in good agreement with previously published literature.[56]

The singly alkyl-substituted naphthoquinone models, namely, methyl- and ethyl-substituted 1,4-naphthoquinone, display a similar trend of electron spin density distribution on the primary ring. Both alkyl substituents cause a decrease in the electron spin density at the carbon atoms at the 3 and 5 positions. The carbon atoms at the other positions display an increase in the electron spin density due to the electron-donating nature of the methyl and ethyl substituent groups. Due to rapid rotation of the methyl groups, the proton hyperfine interactions are averaged and equivalent. For the ethyl substituent, only the hyperfine interactions of the β-methylene protons are observed, as the hyperfine interactions of the terminal methyl protons are too small to be resolved. Both methyl- and ethyl-substituted 1,4-naphthoquinone display equivalent electron spin density on all of the carbon atoms of the primary ring with the exception of the carbon atom at the 2 position. This indicates that, while the initial substitution of the 1,4-naphthoquinone affects the electron spin density distribution throughout the aromatic ring system, a change in the length of the alkyl substituent has minimal effect. This is in agreement with previous literature.[57,58] The doubly alkyl-substituted naphthoquinone, dimethyl 1,4-naphthoquinone, displays a very similar electron spin density distribution in comparison with methyl- and ethyl-substituted 1,4-naphthoquinone.

The dichloro-substituted 1,4-naphthoquinone shows an increase in the electron spin density at all of the carbon atoms on the secondary ring (carbon atoms at positions 5−8). It has been shown through DFT calculations that the addition of an electronegative element (such as chlorine) to a naphthoquinone will alter the electron spin density distribution of the entire molecule.[59] Such an element will cause alternating positive and negative changes in the electron spin density on the carbon atoms of the naphthoquinone ring. It was also shown that the positive changes are larger in magnitude than the negative. In 2,3-dichloro-1,4-naphthoquinone, there are chlorine atoms bound to the carbon atom at the 2 and 3 positions. Each carbon atom of the ring will experience an additive positive and negative change in electron spin density from the chloro substituents. Due to the larger positive component, the net effect is an increase of the electron spin density at each carbon atom. The electron spin density for the carbon atoms at the 2 and 3 positions of the primary ring could not be determined due to the lack of a neighboring α-hydrogen. As with the 2,3-dichloro-1,4-naphthoquinone, the hydroxyl-substituted 1,4-naphthoquinone shows an increase in the electron spin density of the secondary ring carbon atoms at the 6−8 positions. This is in agreement with previously published studies.[60] Similar to the chloro substituents, the oxygen atom of the hydroxyl substituent is expected to induce alternating positive and negative changes in the electron spin density at the carbon atoms of the primary ring of the naphthoquinone.

In vitamin K_1, there are two alkyl substituents, namely, a methyl group and the phytyl chain. The strongest proton hyperfine interaction that is observed is attributed to the methyl group by comparison with 2-methyl-1,4-naphthoquinone. The proton hyperfine interactions of the secondary ring of vitamin K_1 have been assigned by comparison with previously published literature.[61,62] The remaining proton hyperfine interactions that are observed arise from the β-methylene protons at the carbon atom at position 3 of the phytyl group. Since the hyperfine interaction of these protons depends strongly on the orientation of the substituent group, any deviation from symmetry will cause the two β-methylene protons to be inequivalent, with one proton interacting much more strongly than the other due to the larger overlap with the p_Z-orbitals of the quinone ring. In this study, we observe two strong hyperfine interactions that indicate two conformations of the β-methylene protons. Using eq 2 and the electron spin density that was previously obtained from DFT calculations, we determine the angle between the C−H bond of the two strongly coupled β-methylene protons and the axis normal to the quinone ring plane. For the hyperfine coupling values of 4.40 and 3.10 MHz, θ is determined as 48.6 and 56.3°, respectively. We favor the presence of two separate conformations as opposed to inequivalent protons of the same conformation of the β-methylene group. This is because the protons of a β-methylene group are at an angle of 120° from one another and if the symmetry is broken then the two protons are at differing angles from the axis perpendicular to the quinone ring plane. This would cause one of the hyperfine interactions to be significantly stronger than the second hyperfine interaction. However, the observed values of the hyperfine interactions of 4.40 and 3.10 MHz are comparable. Hence, it is concluded that the hyperfine parameters obtained for β-methylene protons do not arise from the same β-methylene group. Instead, these are attributed to different conformations of the β-methylene group that may be caused by steric interference from the neighboring methyl group at the carbon atom at the 2 position, multiple isopropyl groups from the H-bonding solvent, and the H-bonding of one of the β-methylene protons to the carbonyl oxygen atom of the quinone ring which could restrict the movement of the phytyl chain.

2D ^{1}H HYSCORE Spectroscopy of Naphthoquinone Models. The 2D HYSCORE spectroscopy measurements yield a two-dimensional correlation spectrum of the hyperfine interactions between the unpaired electron spin with the surrounding nuclear spins. In comparison with one-dimensional EPR spectroscopy techniques, such as electron nuclear double resonance (ENDOR) and electron spin echo envelope modulation (ESEEM) spectroscopy, the use of two dimensions in HYSCORE spectroscopy increases the frequency space that provides higher resolution. 2D ^{1}H HYSCORE spectroscopy is particularly suitable for measuring strongly anisotropic hyperfine (dipolar) interactions, such as H-bonded protons. In the present study, the 2D ^{1}H HYSCORE spectroscopy experiments are used to observe H-bonding interactions of the naphthosemiquinone models with the solvent molecules. Among other magnetically coupled protons, H-bonded nuclei can be easily identified due to their characteristically large anisotropic dipolar component of the hyperfine interaction. The anisotropic and isotropic hyperfine parameters for the H-bonded proton of the naphthosemiquinone models that are determined by linear analysis are presented in Table 3. For the naphthosemiquinone models with the exception of VK_1 and DMNQ, the anisotropic

hyperfine component, T, is nearly identical ($\sim$2.9 MHz) with less than 10% deviation. The isotropic hyperfine component, a_{iso}, has a near-zero value for all the naphthosemiquinone models.

The relation between the anisotropic dipolar coupling of the H-bonded proton and the strength of the H-bond can be approximated by the point-dipole magnetic interaction:[44]

$$T = \frac{\chi}{r_{HB}^3}\rho_O \qquad (4)$$

where χ is a constant, r is the H-bonding distance, and ρ is the electron spin density at the carbonyl oxygen atom that is participating in the hydrogen bond. The spin density on the carbonyl oxygen atom has been previously determined as 0.20 for both 1,4-naphthoquinone and VK_1.[23] From the results of this study, the H-bond length of the naphthoquinone models is $\sim$1.78 Å and remains conserved through the series. This indicates that the substituents have minimal effects on the strength of the H-bonds of the naphthosemiquinone models. The anisotropic hyperfine parameters and the H-bond lengths that are determined in the present study compare well with previous literature.[22,23,63]

The planarity of a H-bond can be estimated through a direct measure of the electron spin density at the nucleus, a_{iso}.[31,32] When a H-bond is in plane with the ring of the naphthosemiquinone, there is insignificant orbital overlap between the H-bonding partner and the p-orbitals of the carbonyl oxygen atom; thus, the value of a_{iso} is very small. In the case of an out-of-plane H-bond, the spin density is transferred from the p-orbitals of the carbonyl oxygen of the naphthosemiquinone to the p-orbitals of the H-bonding solvent molecule. This in turn causes negative electron spin density on the H-bonding proton that leads to a negative value of a_{iso}.[64] The experimental values of a_{iso} that are obtained in this study (Table 3) show a small absolute value of a_{iso} for all of the model naphthoquinones (-0.5 MHz $< a_{iso} < 0.5$ MHz), with the exception of VK_1 and DMNQ. Thus, we conclude that for all the naphthoquinone models (with the exception of VK_1 and DMNQ) the geometry of H-bonds formed between the carbonyl oxygen atoms and the surrounding solvent molecules is approximately planar with respect to the plane of the primary ring. The substituent groups have a subtle effect on the length and geometry of the H-bonds formed with solvent molecules.

Unlike the majority of the naphthoquinone models, VK_1 and DMNQ present very different results. For both VK_1 and DMNQ naphthosemiquinone radicals, the values of T and a_{iso} are significantly larger in magnitude in comparison with the other naphthosemiquinone models. The significant magnitude and negative sign of a_{iso} provide direct evidence that the geometry of the H-bonds is highly nonplanar. The increase in the value of T does not necessarily reflect the shorter length of the H-bonds, since some of the electron spin density is transferred to the solvent molecule, making a simple point-dipole approximation less accurate. However, on the basis of theoretical calculations, it has been suggested that the anisotropic dipolar interaction increases with an increase in the magnitude of the isotropic hyperfine interaction upon higher nonplanarity of the H-bond.[22] The anisotropic hyperfine interaction that is determined here is in agreement with the average isotropic hyperfine parameters that were obtained in a recent study using DFT calculations of phylloquinone in a protic solvent.[23] The calculations predict four H-bonds with similar but distinct hyperfine coupling parameters. However, we

do not resolve multiple H-bonds in the present study (Figure S3, Supporting Information). In addition, our experimental results indicate a slightly larger (more negative) isotropic coupling, indicating a H-bond geometry that is more out of plane than the model that is predicted by the theoretical DFT calculations. The difference in the H-bond geometry of VK$_1$ and DMNQ is most likely due to significant steric hindrance that is induced by the presence of bulky methyl and methylene groups at the 2 and 3 positions of the primary ring. Interestingly, the presence of a single methyl or methylene group on the primary ring does not result in a significant difference in the planarity of the H-bonds.

Previous 2D ^{1}H HYSCORE studies of the phyllosemiquinone radical, A$_{1A}$$^-$, of PSI have determined that the values of T and a_{iso} are 3.93 and −0.27 MHz, respectively.[31] The value of the isotropic hyperfine interaction, a_{iso}, that is obtained for VK$_1$ in a protic solvent is much larger than the value for A$_{1A}$$^-$ in PSI. This indicates much higher planarity of the H-bond formed between A$_{1A}$$^-$ and Leu722 residue in the protein in comparison with naphthosemiquinones in a protic solvent. This could be due to the restricted conformational freedom within the protein pocket that constrains the H-bond to be more planar *in vivo*.

ASSOCIATED CONTENT

ⓈSupporting Information

The 2D ^{1}H HYSCORE spectra of 5-OHNQ, DCNQ, MNQ, ENQ, DMNQ, and vitamin K$_1$ and the frequency-squared 2D HYSCORE spectra of 1,4-NQ, DCNQ, 5-OHNQ, MNQ, ENQ, DMNQ, and VK$_1$ in IPA. This material is available free of charge via the Internet at http://pubs.acs.org.

AUTHOR INFORMATION

Corresponding Author
*E-mail: lakshk@rpi.edu. Phone: (518) 276 3271. Fax: (518) 276 4887.

Notes
The authors declare no competing financial interest.

ACKNOWLEDGMENTS

REFERENCES

(1) Iwata, S.; Lee, J. W.; Okada, K.; Lee, J. K.; Iwata, M.; Rasmussen, B.; Link, T. A.; Ramaswamy, S.; Jap, B. K. Complete Structure of the 11-Subunit Bovine Mitochondrial Cytochrome bc(1) Complex. *Science* **1998**, *281*, 64−71.

(2) Zhang, Z. L.; Huang, L. S.; Shulmeister, V. M.; Chi, Y. I.; Kim, K. K.; Hung, L. W.; Crofts, A. R.; Berry, E. A.; Kim, S. H. Electron Transfer by Domain Movement in Stockbroker bc(1). *Nature* **1998**, *392*, 677−684.

(3) Xia, D.; Yu, C. A.; Kim, H.; Xian, J. Z.; Kachurin, A. M.; Zhang, L.; Yu, L.; Deisenhofer, J. Crystal Structure of the Cytochrome bc(1) Complex from Bovine Heart Mitochondria. *Science* **1997**, *277*, 60−66.

(4) Boudreaux, B.; MacMillan, F.; Teutloff, C.; Agalarov, R.; Gu, F. F.; Grimaldi, S.; Bittl, R.; Brettel, K.; Redding, K. Mutations in Both Sides of the Photosystem I Reaction Center Identify the Phylloquinone Observed by Electron Paramagnetic Resonance Spectroscopy. *J. Biol. Chem.* **2001**, *276*, 37299−37306.

(5) Lancaster, C. R. D.; Michel, H. Refined Crystal Structures of Reaction Centres from Rhodopseudomonas viridis in Complexes with the Herbicide Atrazine and Two Chiral Atrazine Derivatives Also Lead to a New Model of the Bound Carotenoid. *J. Mol. Biol.* **1999**, *286*, 883−898.

(6) Feher, G.; Allen, J. P.; Okamura, M. Y.; Rees, D. C. Structure and Function of Bacterial Photosynthetic Reaction Centers. *Nature* **1989**, *339*, 111−116.

(7) Deisenhofer, J.; Epp, O.; Miki, K.; Huber, R.; Michel, H. Structure of the Protein Subunits in the Photosynthetic Reaction Center of Rhodopseudomonas viridis at 3 Å Resolution. *Nature* **1985**, *318*, 618−624.

(8) Zouni, A.; Witt, H. T.; Kern, J.; Fromme, P.; Krauss, N.; Saenger, W.; Orth, P. Crystal Structure of Photosystem II from Synechococcus elongatus at 3.8 Angstrom Resolution. *Nature* **2001**, *409*, 739−743.

(9) Umena, Y.; Kawakami, K.; Shen, J. R.; Kamiya, N. Crystal Structure of Oxygen-Evolving Photosystem II at a Resolution of 1.9 Angstrom. *Nature* **2011**, *473*, 55−U65.

(10) Krauss, N.; Schubert, W. D.; Klukas, O.; Fromme, P.; Witt, H. T.; Saenger, W. Photosystem I at 4 Angstrom Resolution Represents the First Structural Model of a Joint Photosynthetic Reaction Centre and Core Antenna System. *Nat. Struct. Biol.* **1996**, *3*, 965−973.

(11) Jordan, P.; Fromme, P.; Witt, H. T.; Klukas, O.; Saenger, W.; Krauss, N. Three-Dimensional Structure of Cyanobacterial Photosystem I at 2.5 Angstrom Resolution. *Nature* **2001**, *411*, 909−917.

(12) Ferreira, K. N.; Iverson, T. M.; Maghlaoui, K.; Barber, J.; Iwata, S. Architecture of the Photosynthetic Oxygen-Evolving Center. *Science* **2004**, *303*, 1831−1838.

(13) Loll, B.; Kern, J.; Saenger, W.; Zouni, A.; Biesiadka, J. Towards Complete Cofactor Arrangement in the 3.0 Angstrom Resolution Structure of Photosystem II. *Nature* **2005**, *438*, 1040−1044.

(14) Kamiya, N.; Shen, J. R. Crystal Structure of Oxygen-Evolving Photosystem II from Thermosynechococcus vulcanus at 3.7 Angstrom Resolution. *Proc. Natl. Acad. Sci. U.S.A.* **2003**, *100*, 98−103.

(15) Brettel, K.; Leibl, W. Electron Transfer in Photosystem I. *Biochim. Biophys. Acta, Bioenerg.* **2001**, *1507*, 100−114.

(16) Ptushenko, V. V.; Cherepanov, D. A.; Krishtalik, L. I.; Semenov, A. Y. Semi-Continuum Electrostatic Calculations of Redox Potentials in Photosystem I. *Photosynth. Res.* **2008**, *97*, 55−74.

(17) Dutton, P. L.; Leigh, J. S.; Wraight, C. A. Direct Measurement of Midpoint Potential of Primary Electron-Acceptor in Rhodopseudomonas-Spheroides In-Situ and in Isolated State - Some Relationships with pH and Ortho-Phenanthroline. *FEBS Lett.* **1973**, *36*, 169−173.

(18) Rutherford, A. W.; Evans, M. C. W. Direct Measurement of the Redox Potential of the Primary and Secondary Quinone Electron-Acceptors in Rhodopseudomonas sphaeroides (Wild-Type) by Electron Paramagnetic Resonance Spectrometry. *FEBS Lett.* **1980**, *110*, 257−261.

(19) Golbeck, J. H.; Kok, B. Redox Titration of Electron-Acceptor Q and the Plastoquinone Pool in Photosystem II. *Biochim. Biophys. Acta* **1979**, *547*, 347−360.

(20) Krieger, A.; Rutherford, A. W.; Johnson, G. N. On the Determination of Redox Midpoint Potential of the Primary Quinone Electron-Acceptor, Q(A), in Photosystem II. *Biochim. Biophys. Acta, Bioenerg.* **1995**, *1229*, 193−201.

(21) Srinivasan, N.; Golbeck, J. H. Protein-Cofactor Interactions in Bioenergetic Complexes: The Role of the A(1A) and A(1B) Phylloquinones in Photosystem I. *Biochim. Biophys. Acta, Bioenerg.* **2009**, *1787*, 1057−1088.

(22) O'Malley, P. J. Density Functional Calculated Spin Densities and Hyperfine Couplings for Hydrogen Bonded 1,4-Naphthosemiquinone and Phyllosemiquinone Anion Radicals: A Model for the A(1) Free Radical Formed in Photosystem I. *Biochim. Biophys. Acta, Bioenerg.* **1999**, *1411*, 101−113.

(23) Epel, B.; Niklas, J.; Sinnecker, S.; Zimmermann, H.; Lubitz, W. Phylloquinone and Related Radical Anions Studied by Pulse Electron Nuclear Double Resonance Spectroscopy at 34 GHz and Density Functional Theory. *J. Phys. Chem. B* **2006**, *110*, 11549−11560.

(24) Pushkar, Y. N.; Zech, S. G.; Stehlik, D.; Brown, S.; van der Est, A.; Zimmermann, H. Orientation and Protein-cofactor Interactions of Monosubstituted n-Alkyl Naphthoquinones in the A(1) Binding Site of Photosystem I. *J. Phys. Chem. B* **2002**, *106*, 12052−12058.

(25) Sinnecker, S.; Flores, M.; Lubitz, W. Protein-Cofactor Interactions in Bacterial Reaction Centers from Rhodobacter sphaeroides R-26: Effect of Hydrogen Bonding on the Electronic and Geometric Structure of the Primary Quinone. A Density Functional Theory Study. *Phys. Chem. Chem. Phys.* **2006**, *8*, 5659–5670.

(26) Ishikita, H.; Knapp, E. W. Control of Quinone Redox Potentials in Photosystem II: Electron Transfer and Photoprotection. *J. Am. Chem. Soc.* **2005**, *127*, 14714–14720.

(27) Breton, J.; Boullais, C.; Burie, J. R.; Nabedryk, E.; Mioskowski, C. Binding-Sites of Quinones in Photosynthetic Bacterial Reaction Centers Investigated by Light-Induced FTIR Difference Spectroscopy - Assignment of the Interactions of Each Carbonyl of Q(A) in Rhodobacter sphaeroides Using Site-Specific C-13 Labeled Ubiquinone. *Biochemistry* **1994**, *33*, 14378–14386.

(28) Breton, J.; Burie, J. R.; Berthomieu, C.; Berger, G.; Nabedryk, E. Binding-Sites of Quinones in Photosynthetic Bacterial Reaction Centers Investigated by Light-Induced FTIR Difference Spectroscopy - Assignment of the Q(A) Vibrations in Rhodobacter sphaeroides Using O-18 Labeled or C-13 Labeled Ubiquinone and Vitamin K1. *Biochemistry* **1994**, *33*, 4953–4965.

(29) Deligiannakis, Y.; Rutherford, A. W. Electron Spin Echo Envelope Modulation Spectroscopy in Photosystem I. *Biochim. Biophys. Acta, Bioenerg.* **2001**, *1507*, 226–246.

(30) Kolling, D. R. J.; Samoilova, R. I.; Holland, J. T.; Berry, E. A.; Dikanov, S. A.; Crofts, A. R. Exploration of Ligands to the Q(i) Site Semiquinone in the bc(1) Complex Using High-Resolution EPR Spectroscopy. *J. Biol. Chem.* **2003**, *278*, 39747–39754.

(31) Srinivasan, N.; Chatterjee, R.; Milikisiyants, S.; Golbeck, J. H.; Lakshmi, K. V. Effect of Hydrogen Bond Strength on the Redox Properties of Phylloquinones: A Two-Dimensional Hyperfine Sublevel Correlation Spectroscopy Study of Photosystem I. *Biochemistry* **2011**, *50*, 3495–3501.

(32) Chatterjee, R.; Milikisiyants, S.; Coates, C. S.; Lakshmi, K. V. High-Resolution Two-Dimensional H-1 and N-14 Hyperfine Sublevel Correlation Spectroscopy of the Primary Quinone of Photosystem II. *Biochemistry* **2011**, *50*, 491–501.

(33) Sinnecker, S.; Reijerse, E.; Neese, F.; Lubitz, W. Hydrogen Bond Geometries from Electron Paramagnetic Resonance and Electron-nuclear Double Resonance Parameters: Density Functional Study of Quinone Radical Anion-Solvent Interactions. *J. Am. Chem. Soc.* **2004**, *126*, 3280–3290.

(34) Beal, D.; Rappaport, F.; Joliot, P. A New High-Sensitivity 10 ns Time-Resolution Spectrophotometric Technique Adapted to In Vivo Analysis of the Photosynthetic Apparatus. *Rev. Sci. Instrum.* **1999**, *70*, 202–207.

(35) Joliot, P.; Joliot, A. In Vivo Analysis of the Electron Transfer within Photosystem I: Are the Two Phylloquinones Involved? *Biochemistry* **1999**, *38*, 11130–11136.

(36) Setif, P.; Brettel, K. Forward Electron-Transfer from Phylloquinone-A(1) to Iron-Sulfur Centers in Spinach Photosystem I. *Biochemistry* **1993**, *32*, 7846–7854.

(37) Brettel, K. Electron Transfer from Acceptor A(1) to the Iron-Sulfur Clusters in Photosystem I Measured with a Time Resolution of 2 ns. *Photosynth.: Mech. Eff., Vols I-V* **1998**, 611–614.

(38) Johnson, T. W.; Zybailov, B.; Jones, A. D.; Bittl, R.; Zech, S.; Stehlik, D.; Golbeck, J. H.; Chitnis, P. R. Recruitment of a Foreign Quinone into the A(1) Site of Photosystem I - In Vivo Replacement of Plastoquinone-9 by Media Supplemented Naphthoquinones in Phylloquinone Biosynthetic Pathway Mutants of Synechocystis sp PCC 6803. *J. Biol. Chem.* **2001**, *276*, 39512–39521.

(39) Mula, S.; Savitsky, A.; Mobius, K.; Lubitz, W.; Golbeck, J. H.; Mamedov, M. D.; Semenov, A. Y.; van der Est, A. Incorporation of a High Potential Quinone Reveals That Electron Transfer in Photosystem I Becomes Highly Asymmetric at Low Temperature. *Photochem. Photobiol. Sci.* **2012**, *11*, 946–956.

(40) Daniele, S.; Baldo, M. A.; Bragato, C. A Steady-State Voltammetric Investigation on the Oxidation of Ferrocene in Ethanol-Water Mixtures. *Electrochem. Commun.* **1999**, *1*, 37–41.

(41) Connelly, N. G.; Geiger, W. E. Chemical Redox Agents for Organometallic Chemistry. *Chem. Rev.* **1996**, *96*, 877–910.

(42) Bard, A. J.; Faulkner, L. R. *Electrochemical Methods: Fundamentals and Applications*; Oxford University Press: New York, 2001.

(43) Stoll, S.; Schweiger, A.; Easy Spin, A. Comprehensive Software Package for Spectral Simulation and Analysis in EPR. *J. Magn. Reson.* **2006**, *178*, 42–55.

(44) Schweiger, A.; Jeschke, G. *Principles of Pulse Electron Paramagnetic Resonance*; Oxford University Press: New York, 2001.

(45) McConnell, H. M.; Chesnut, D. B. Theory of Isotropic Hyperfine Interactions in pi-Electron Radicals. *J. Chem. Phys.* **1958**, *28*, 107–117.

(46) McConnell, H. M. Indirect Hyperfine Interactions in the Paramagnetic Resonance Spectra of Aromatic Free Radicals. *J. Chem. Phys.* **1956**, *24*, 764–766.

(47) Barton, B. L.; Fraenkel, G. K. Electron Spin Resonance Spectra of Methyl-Substituted Dihydropyrazine Cations and Related Radicals. *J. Chem. Phys.* **1964**, *41*, 1455.

(48) McLachlan, A. D. Hyperconjugation in the Electron Resonance Spectra of Free Radicals. *Mol. Phys.* **1958**, *1*, 233–240.

(49) Das, M. R.; Connor, H. D.; Leniart, D. S.; Freed, J. H. An Electron Nuclear Double Resonance and Electron Spin Resonance Study of Semiquinones Related to Vitamin-K and Vitamin-E. *J. Am. Chem. Soc.* **1970**, *92*, 2258–2268.

(50) Dikanov, S. A.; Bowman, M. K. Cross-Peak Lineshape of Two-Dimensional ESEEM Spectra in Disordered S = 1/2, I = 1/2 Spin Systems. *J. Magn. Reson., Ser. A* **1995**, *116*, 125–128.

(51) Rahman, A.; Qureshi, R.; Ahmed, S. Electrochemical and Computational Interpretations of Hydrogen-Bonding of Naphthoquinones with Methanol. *J. Chem. Soc. Pak.* **2008**, *30*, 655–663.

(52) Weyers, A. M.; Chatterjee, R.; Milikisiyants, S.; Lakshmi, K. V. Structure and Function of Quinones in Biological Solar Energy Transduction: A Differential Pulse Voltammetry, EPR, and Hyperfine Sublevel Correlation (HYSCORE) Spectroscopy Study of Model Benzoquinones. *J. Phys. Chem. B* **2009**, *113*, 15409–15418.

(53) Bauscher, M.; Mantele, W. Electrochemical and Infrared Spectroscopic Characterization of Redox Reactions of p-Quinones. *J. Phys. Chem.* **1992**, *96*, 11101–11108.

(54) Gupta, N.; Linschitz, H. Hydrogen-Bonding and Protonation Effects in Electrochemistry of Quinones in Aprotic Solvents. *J. Am. Chem. Soc.* **1997**, *119*, 6384–6391.

(55) Broze, M.; Luz, Z.; Silver, B. L. Oxygen-17 Hyperfine Splitting Constants in ESR Spectra of p-Semiquinones-17O. *J. Chem. Phys.* **1967**, *46*, 4891–4902.

(56) Stone, E. W.; Maki, A. H. Electron Spin Resonance of Semiquinones in Aprotic Solvents. *J. Chem. Phys.* **1962**, *36*, 1944–1945.

(57) Spoyalov, A. P.; Samoilova, R. I.; Tyryshkin, A. M.; Dikanov, S. A.; Liu, B. L.; Hoff, A. J. ENDOR and ESEEM Studies of Ion Radicals of Artificial Dimethoxy-1,4-benzoquinone or Halogen-1,4-benzoquinones with an Alkyl Side-Chain of Differing Length. *J. Chem. Soc., Perkin Trans.* **1992**, 1519–1524.

(58) Piette, L. H.; Okamura, M.; Rabold, G. P.; Ogata, R. T.; Moore, R. E.; Scheuer, P. J. High-Resolution Electron Spin Resonance Studies of Hyperfine Interactions in Substituted 1,4-Naphthoquinones and Naphthazarins. *J. Phys. Chem.* **1967**, *71*, 29.

(59) van der Est, A.; Pushkar, Y.; Karyagina, I.; Fonovic, B.; Dudding, T.; Niklas, J.; Lubitz, W.; Golbeck, J. H. Incorporation of 2,3-Disubstituted-1,4-naphthoquinones into the A(1) Binding Site of Photosystem I Studied by EPR and ENDOR Spectroscopy. *Appl. Magn. Reson.* **2010**, *37*, 65–83.

(60) Hernandez-Munoz, L. S.; Gomez, M.; Gonzalez, F. J.; Gonzalez, I.; Frontana, C. Towards a Molecular-Level Understanding of the Reactivity Differences for Radical Anions of Juglone and Plumbagin: An Electrochemical and Spectroelectrochemical Approach. *Org. Biomol. Chem.* **2009**, *7*, 1896–1903.

(61) Bowman, M. K.; Thurnauer, M. C.; Norris, J. R.; Dikanov, S. A.; Gulin, V. I.; Tyryshkin, A. M.; Samoilova, R. I.; Tsvetkov, Y. D.

Characterization of Free Radicals from Vitamin K-1 and Menadione by 2 mm-Band EPR, ENDOR and ESEEM. *Appl. Magn. Reson.* **1992**, *3*, 353−368.

(62) Fritsch, J. M.; Tatwawad., Sv; Adams, R. N. Electron Paramagnetic Resonance Studies of Vitamin K and Vitamin E. *J. Phys. Chem.* **1967**, *71*, 338−342.

(63) Kaupp, M.; Remenyi, C.; Vaara, J.; Malkina, O. L.; Malkin, V. G. Density Functional Calculations of Electronic g-Tensors for Semiquinone Radical Anions. The Role of Hydrogen Bonding and Substituent Effects. *J. Am. Chem. Soc.* **2002**, *124*, 2709−2722.

(64) O'Malley, P. J. A Density Functional Study of the Effect of Orientation of Hydrogen Bond Donation on the Hyperfine Couplings of Benzosemiquinones: Relevance to Semiquinone-Protein Hydrogen Bonding Interactions In Vivo. *Chem. Phys. Lett.* **1998**, *291*, 367−374.

(65) Niklas, J.; Epel, B.; Antonkine, M.; Sinnecker, S.; Pandelia, M.; Lubitz, W. Electronic Structure of the Quinone Radical Anion $A1^{\bullet-}$ of Photosystem I Investigated by Advanced Pulse EPR and ENDOR Techniques. *J. Phys. Chem. B.* **2009**, *131*, 10367−10379.